

Boise State University

**ScholarWorks**

---

Geosciences Faculty Publications and  
Presentations

Department of Geosciences

---

3-2022

## **Developing a Soil Column System to Measure Hydrogeophysical Properties of Unconsolidated Sediment**

Taylor Bienvenue  
*Boise State University*

Jing Xie  
*Boise State University*

Qifei Niu  
*Boise State University*

—

# Developing a soil column system to measure hydrogeophysical properties of unconsolidated sediment

Taylor Bienvenue<sup>1</sup> | Jing Xie<sup>1,2</sup> | Qifei Niu<sup>1</sup> 

<sup>1</sup> Dep. of Geosciences, Boise State Univ., Boise, ID 83725-1535, USA

<sup>2</sup> School of Geoscience and Info-Physics, Central South Univ., Changsha, Hunan, China

## Correspondence

Qifei Niu, Dep. of Geosciences, Boise State Univ., Boise, ID, 83725-1535, USA.  
Email: [qifeiniu@boisestate.edu](mailto:qifeiniu@boisestate.edu)

Assigned to Associate Editor Sarah Garré.

## Funding information

American Chemicals Society, Grant/Award Number: PRF#60925-DNI9

## Abstract

Geophysical methods have been increasingly used to characterize the Earth's critical zone (CZ) and monitor hydrological processes occurring within it. For a quantitative interpretation, geophysical studies of CZ materials are necessary, and thus require more sophisticated laboratory setups. In this study, we develop a hydrogeophysical soil column system to measure key hydraulic and electrical properties of regolith in CZs. The developed soil column system consists of two components: (a) a novel hydrogeophysical probe that measures pore water pressure and electrical potential in soils and (b) a cylindrical cell to hold soil samples. The system can be arranged to perform both saturated flow and drainage tests. The saturated flow test is similar to the traditional constant head experiment for determining the hydraulic conductivity and streaming potential coupling coefficient. The drainage tests can produce transient responses of cumulative overflow, pore water pressure, and streaming potential. These transient data can be used to estimate the sample's electrical and hydraulic properties with the coupled, stochastic hydrogeophysical inversion. A sand sample is used to demonstrate the procedures of applying this new system. The measured saturated hydraulic conductivity and streaming potential coupling coefficient of the sand are within the typical ranges of sands reported in the literature. The inversion-estimated soil parameters can well reproduce the measured transient responses during the drainage test of the sample. Moreover, the inversion-estimated saturated properties are in good agreement with those independently measured in the saturated flow test, showing the robustness of the developed system.

## 1 | INTRODUCTION

The subsurface portion of the critical zone (CZ) plays a vital role in regulating groundwater's amount, routing, and residence time (Brooks et al., 2015). To have a predictive understanding of hydrological processes in CZs, we need to charac-

terize the spatial distributions of hydraulic states and properties in the subsurface, such as water content, permeability, and soil water retention characteristics. The most commonly used method for hydrologic characterization is probably field sampling and then testing in the laboratory (e.g., Wieting et al., 2017). Soil pits are usually dug, or drilling is performed to collect soil/rock samples, which can be tested in the laboratory. Important hydraulic properties can be either directly measured with the collected samples or estimated using

**Abbreviations:** CI, confidence interval; CZ, critical zone; SP, self-potential; SWRC, soil water retention curve.

This is an open access article under the terms of the [Creative Commons Attribution](https://creativecommons.org/licenses/by/4.0/) License, which permits use, distribution and reproduction in any medium, provided the original work is properly cited.

© 2022 The Authors. *Vadose Zone Journal* published by Wiley Periodicals LLC on behalf of Soil Science Society of America

pedotransfer functions with some easy-to-measure properties as input (Wösten et al., 2001). Most CZs are heterogeneous laterally and vertically due to complex interactions between the bedrock, vegetation, climate, and water (e.g., Lin, 2010). To achieve a high-resolution characterization, we usually need to collect and test many samples, which are costly and thus prohibitive for most CZ studies.

Strong correlations between hydraulic states/properties and some geophysical measurements have been observed in many geological materials (Lesmes & Friedman, 2005). For instance, water content is a primary factor affecting a soil's dielectric property (Topp et al., 1980), nuclear magnetic resonance signal (e.g., Paetzold et al., 1985), and electrical resistivity (Archie, 1942); the hydraulic conductivity of sediments have been found to correlate with their formation factor and imaginary conductivity (e.g., Weller et al., 2015). Due to these correlations, it becomes increasingly popular to use geophysical methods to characterize the hydraulic properties of the subsurface (Binley et al., 2015). Moreover, if geophysical tests are conducted repeatedly over a period of time (i.e., time-lapse test), hydrological processes occurring in the subsurface can also be studied (e.g., Robinson et al., 2009). In addition to time-lapse geophysical tests, subsurface water dynamics may also be directly sensed by the self-potential (SP) method, which measures the natural occurrence of electrical fields. In hydrological settings, the measured SP signals are correlated with groundwater flux through electrokinetics (Jouniaux et al., 2009).

To successfully apply geophysical methods to CZ hydrology, we need to understand the petrophysical relationships that link geophysical responses of CZ materials to their hydraulic states/properties. Our existing petrophysical knowledge of geological media (Lesmes & Friedman, 2005) is mainly gained in soil science and petroleum engineering. In soil science, petrophysical studies focus on agricultural soils, of which the texture and mineralogy are usually similar within a relatively large field (e.g., Blanchy et al., 2020). In petroleum engineering, reservoir rocks usually have a similar texture or mineralogy within a particular formation (e.g., Han et al., 2015). However, the materials in CZs are distinct in texture and geochemistry even within a thin layer because of the influence of physical and chemical weathering (e.g., Hayes et al., 2019). Currently, our petrophysical understanding of CZ materials is still limited.

One factor prohibiting petrophysical studies of CZ materials is the lack of appropriate laboratory setups that can simultaneously measure the geophysical and hydraulic properties of a sample. Traditional lab setups can only measure a single property of the sample, and measuring multiple properties will need to involve several lab setups. Thus, the material needs to be prepared several times for different tests. For unconsolidated sediments (e.g., materials in the regolith of CZs), it is challenging to maintain the same texture and struc-

### Core Ideas

- A novel hydrogeophysical probe is developed to measure both pore water pressure and electrical potential in soils.
- The new probes are integrated into a soil column to determine key hydrogeophysical properties of soils.
- Experimental results of a sand sample show the effectiveness and robustness of the integrated soil column system.

ture for all the samples in different lab tests. Note that textural and structural variations in different samples of a geological material could adversely affect the determination of the hydrogeophysical relationship of the material (Niu et al., 2015). Therefore, it is always preferred if both geophysical and hydraulic tests can be conducted on one sample using a single lab setup.

More importantly, most CZs have a large portion that is above the groundwater table. Thus, a good lab setup should be able to control the hydraulic states (i.e., water content/soil water tension) of a material such that the geophysical responses in unsaturated conditions can also be measured. In practice, special instruments (e.g., the pressure plate apparatus) are needed to control the hydraulic states (e.g., Wu et al., 2017), making the geophysical measurement of unsaturated soils burdensome. Also, some geoelectrical experiments such as complex electrical conductivity and SP measurements often use nonpolarizing electrodes, which need to be fully immersed in water to give a reliable electrical potential reading. However, these electrodes may lose contact with the pore water in unsaturated conditions if directly inserted into the sample (e.g., Linde et al., 2007). To advance our petrophysical understanding of CZ materials, it is therefore critical to develop new laboratory setups to address the abovementioned problems.

This study aims to develop a soil column system that can simultaneously measure the key hydraulic and electrical properties of unconsolidated materials in both saturated and unsaturated conditions. The electrical properties considered here include the streaming potential coupling coefficient and complex conductivity. In porous geological media, the mineral surface is usually (negatively) charged (e.g., Sposito et al., 1999; Yin et al., 2012); when in contact with the electrolyte, the electrical double layer (EDL) forms at the water–mineral interface. The pore water flow can drag a portion of the excess ions in the EDL, producing the so-called streaming potential (Revil & Jardani, 2013). The streaming potential coupling coefficient quantifies a material's ability to generate

streaming potential (e.g., Jaafar et al., 2009). For saturated materials, the coupling coefficient is usually measured with the constant head flow experiment (e.g., Jackson & Vinogradov, 2012; Vinogradov et al., 2010); for unsaturated materials, the coupling coefficient is often measured indirectly with the transient flow experiment (e.g., Allègre, et al., 2010; Guichet et al., 2003; Jougnot & Linde, 2013; Mboh et al., 2012). Due to the direct coupling between water flow and electrical current flow, streaming potential measurements have been used in hydrology, for example, to detect preferential infiltration pathway (Jardani et al., 2007), reconstruct groundwater table (Jardani et al., 2009), and characterize stream-aquifer exchanges (Valois et al., 2018).

The real component of the complex conductivity, which is similar to the electrical conductivity measured using direct current, quantifies a material's ability to conduct electricity; the imaginary conductivity is associated with the material's ability to store energy. The complex conductivity of saturated and unsaturated geological materials has been extensively studied (e.g., Breede et al., 2011, 2012; Lesmes & Friedman, 2005; Ulrich & Slater, 2004). It has been found that both the real and imaginary conductivity of porous geological materials correlate with their hydraulic conductivity (Doussan & Ruy, 2009; Revil & Florsch, 2010; Slater et al., 2014; Slater & Lesmes, 2002; Urish, 1981). These hydraulic-electrical relationships have been used to determine the distribution of hydraulic conductivity at the field scale (e.g., Attwa & Günther, 2013; Hördt et al., 2009).

This paper is organized as follows. We first describe the design of the soil column system, which includes a novel hydrogeophysical probe that can measure both pore water pressure and electrical potential in unconsolidated materials. We then use a sand sample to demonstrate the determination of the sand's various hydraulic and electrical properties with the developed system. Finally, the experimental results are presented, and the estimated soil parameters are analyzed to show the effectiveness of the developed lab setup. Major conclusions are presented at the end of this paper.

## 2 | SOIL COLUMN SYSTEM

This section introduces the proposed soil column system, consisting of two major components: a novel hydrogeophysical probe to measure electrical potential and pore water pressure and a cylindrical cell to hold soil samples. Different arrangements of the soil column system are also introduced for different measurement purposes.

### 2.1 | Novel hydrogeophysical probe

One key component of the soil column system is a novel hydrogeophysical probe, which integrates the nonpolarizing

electrode into a traditional tensiometer. Figure 1 shows a schematic and a prototype of such a probe. As shown in the figure, the probe's tip is a ceramic cup (Location 4 in Figure 1b) with a high air entry value. In unsaturated conditions, the ceramic cup will prevent air in the soil from entering into the probe when soil suction is lower than the air entry value of the ceramic cup. Water, on the other hand, can move quickly between the probe and soil sample, and thus the soil water pressure is always in equilibrium with the water pressure in the probe. Therefore, the pressure transducer inserted into the probe (Location 1 in Figure 1b) can measure the pore water pressure in the sample.

A nonpolarizing Ag/AgCl electrode (Location 3 in Figure 1b) is also inserted into the probe and sealed by a rubber stopper. Due to the presence of the ceramic cup, the probe will always be full of water, ensuring that the electrode is immersed in water even the sample under test is in unsaturated condition (e.g., Ulrich & Slater, 2004). In the probe, an air release point is designed (Location 2 in Figure 1b), which allows for water to be refilled if air diffuses into the tube of the probe. Using ceramic cups with a high air entry value is common in both unsaturated geoelectrical measurement (e.g., Breede et al., 2011) and soil suction measurement (e.g., Take & Bolton, 2003). However, to the best of our knowledge, such an integrated design is not found in previous studies. The obvious advantage of the hydrogeophysical probe is that pore water pressure and electrical potential in soils can be measured in both saturated and unsaturated conditions.

Similar to some previous studies (e.g., Mboh et al., 2012), the hydrogeophysical probe is filled with water from the sample (see section 3.3). Using the same fluid will avoid generating an ionic concentration gradient between the probe and the sample, which can generate a perturbation to the measured SP signals (Jougnot & Linde, 2013). Because a large portion of the probes is outside of the soil sample, the temperature fluctuation in the laboratory could affect the probe's water temperature, thus affecting the performance of Ag/AgCl electrodes (Jougnot & Linde, 2013). Therefore, it is necessary to monitor the water temperature in the probe during an experiment.

### 2.2 | Cylindrical cell and accessories

A cylindrical cell is created using resin with 3-D printing technology (Figure 2). The inner dimensions of the cell are 21 cm in height and 7.5 cm in diameter. Threaded fittings are installed at the top and bottom of the cell to serve as an inlet/outlet for water flow (Figure 2). At 4.5 and 16.5 cm from the bottom of the cell are female pipe threads that allow hydrogeophysical probes to be threaded into the sidewall of the cell (Figure 2a). Adjacent to the hydrogeophysical probes, traditional Ag/AgCl reference electrodes (R0305, Tianjin Aida, Inc.) are also inserted into tubes connected to the sample (Figure 2a). Note that the water in the tubes of traditional

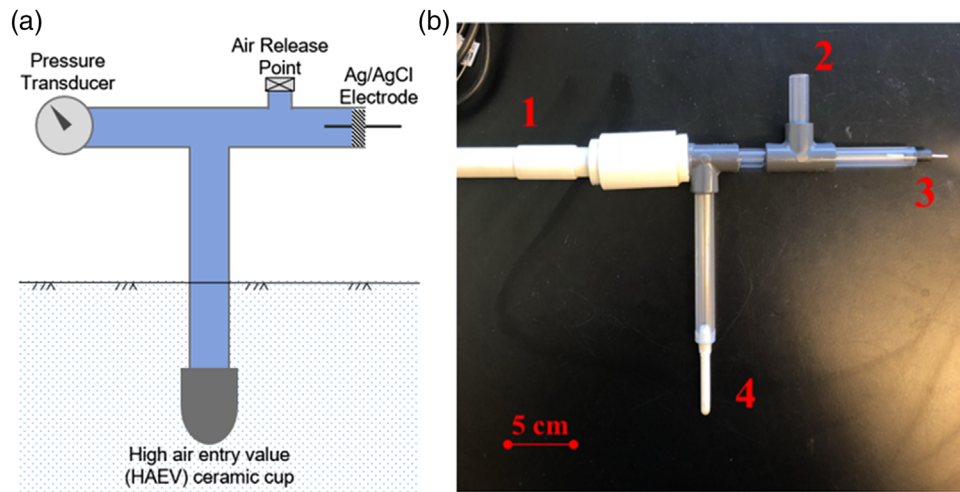


**FIGURE 1** The hydrogeophysical probe proposed in this study: (a) the schematic and (b) a prototype. 1, pressure transducer that measures soil pore water pressure; 2, air release point; 3, nonpolarizing Ag/AgCl electrode; 4, porous ceramic cup with a high air entry value

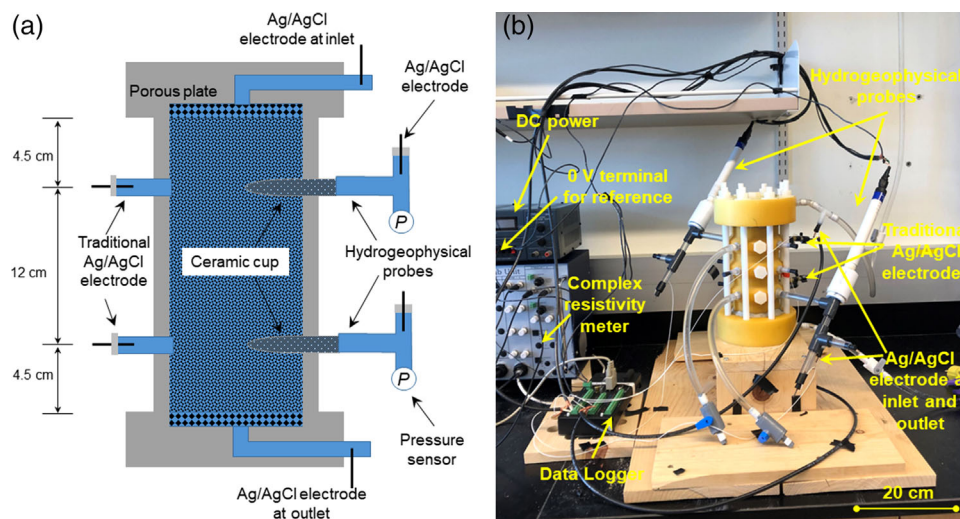


**FIGURE 2** The proposed soil column system: (a) the schematic and (b) the soil column used in this study and auxiliary devices for geoelectrical measurement, including the novel hydrogeophysical probe, traditional Ag/AgCl nonpolarizing electrodes, a data logger, and a complex resistivity meter

Ag/AgCl electrodes will be drained when the sample becomes unsaturated. Thus, these traditional Ag/AgCl electrodes may not measure the electrical responses in a transient flow experiment. All the pressure transducers and electrodes attached to this cell are connected to a data logger (CR1000x, Campbell Scientific, Inc.) via coaxial cables to record the soil water pressure and electrical potentials.

### 2.3 | Arrangement for complex conductivity tests in saturated conditions

The cell and attached probes can be arranged to measure the complex conductivity  $\sigma_{\text{sat}}^*$  of a sample in saturated conditions using the four-electrode technique (e.g., Klein & Santamarina,

1997). In such a test, two metallic plates (e.g., copper) are put at the top and bottom of the sample, and they will be used as current electrodes to inject electrical current into the sample. The induced electrical potential at two different depths of the sample can be measured with the hydrogeophysical probes. Alternatively, the electrical current can be injected through the inlet and outlet of the cell, and electrical potential can be measured by the installed hydrogeophysical probes or traditional nonpolarizing electrodes at different heights. The second arrangement will avoid the placement of metallic plates in the cell and thus eliminate the so-called electrode polarization (e.g., Yang et al., 2018). Additionally, in electrical resistivity measurement, the chemical reaction occurring at the interface between metallic plates and pore water will release ions into the pore water, affecting the pore water chemistry and thus the

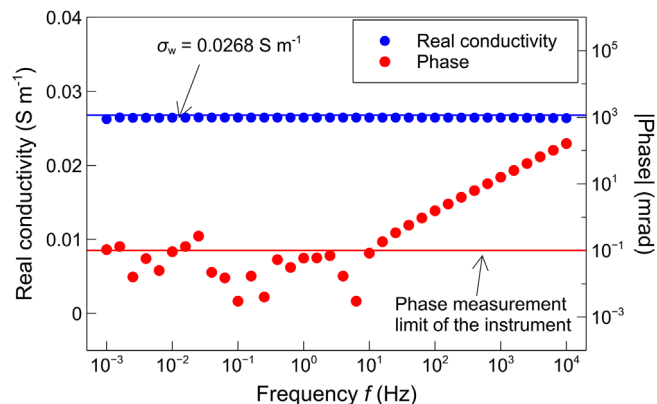


**FIGURE 3** The measured real conductivity and phase of tap water with our developed soil column and hydrogeophysical probes. The water conductivity is also measured independently with a water conductivity meter as  $0.0268 \text{ S m}^{-1}$  (blue solid line). The measured phase are presented as absolute values and the phase detection limit of the instrument is  $\sim 0.1 \text{ mrad}$  (red solid line)

pore water conductivity. Thus, the second method is generally preferred in practice. Note that the second arrangement may not work for unsaturated soils because the electrodes at the inlet/outlet may lose connection with the unsaturated soils. Prior to applying this system to soil samples, we used it to measure the complex conductivity of tap water, and the measured water conductivity and phase are shown in Figure 3. In a broad frequency range ( $10^{-3} \text{ Hz}$  to  $10^4 \text{ Hz}$ ), the water conductivity  $\sigma_w$  can be accurately determined (Figure 3). In the frequency range between  $10^{-3} \text{ Hz}$  and  $10^1 \text{ Hz}$ , the measured phase (absolute value) is generally lower than  $0.1 \text{ mrad}$ , the phase detection limit of the instrument. At frequencies higher than  $10^2 \text{ Hz}$ , the phase increases with frequency, and the values are comparable to other similar studies (e.g., Joseph et al., 2016; Koch et al., 2011). This calibration test shows the accuracy of our developed system in measuring the complex conductivity of materials.

## 2.4 | Arrangement for flow and self-potential test in saturated conditions

The developed soil column system can also be arranged to measure the saturated hydraulic conductivity  $K_{\text{sat}}$  and streaming potential coupling coefficient  $C_{\text{sat}}$  of unconsolidated sediments. As shown in Figure 4, an upper reservoir and a lower reservoir with a constant head are connected to the soil column through pipes to apply a hydraulic gradient across the sample. The upper reservoir keeps water at a constant level of  $\sim 1.3 \text{ m}$  above the top of the soil column. The valves near the inlet and outlet of the soil column can be used to adjust the hydraulic gradient applied to the sample. The flow rate can also be adjusted by changing the height of the lower reser-

voir relative to the soil column. This arrangement is generally similar to the traditional constant head setup for  $K_{\text{sat}}$  measurement (e.g., Mitchell & Soga, 2005). During the test, water will move from the upper reservoir into the sample and then to the lower reservoir, eventually reaching the storage reservoir. These reservoirs are built using acrylic and plastic materials and are connected via vinyl tubing. Metal may influence the complex conductivity and SP measurements and is avoided during the construction of the setup.

This lower constant head reservoir also serves as a point of access to collect water cycled through the sample. The volume of water collected over a short period of time can be used to calculate the flow rate and make water chemistry measurements (e.g., water conductivity  $\sigma_w$  and pH). When water is not being collected from the lower reservoir, it drains into a storage reservoir. Water from the storage reservoir is pumped to an upper constant head reservoir above the soil column with a magnetic drive pump (Little Giant 115V, Franklin Electric, Inc.). A magnetic drive pump eliminates water contact with the pump motor and limits the risk of any water contamination during testing.

One major advantage of the setup is that  $K_{\text{sat}}$ ,  $C_{\text{sat}}$ , and  $\sigma_{\text{sat}}^*$  can be measured on a single sample. These measurements provide a direct way to calculate the volumetric excess charge density (Jougnot et al., 2020), which is a better parameter quantifying the ability of geological material to generate streaming potential. To the best of our knowledge, such an integrated setup is not available for unconsolidated geological materials.

## 2.5 | Arrangement for drainage tests

In addition to saturated flows, soil water pressure and SP signal induced by unsaturated flows can also be measured with the hydrogeophysical probes in a drainage test. Figure 5 shows the arrangement of the soil column system for such a test. After the saturated test is finished, the lower constant head reservoir is moved to a point  $\sim 60 \text{ cm}$  below the soil column (Figure 5). In arranging the system, the valve at the top of the soil column is open, but the bottom valve is closed to maintain saturated conditions for the sample. The drainage test will be initiated once the bottom valve is opened, and then water in the sample starts to flow into the lower constant head reservoir. In the test, the outflow is collected in a container. The weight change of the container will be monitored with a high precision digital balance (Scout SPX622, OHAUS Corporation). Using the monitoring data, we may calculate the water flow rate. In this study, the balance records the cumulative water drained from the soil column with a  $0.01 \text{ g}$  precision. The balance is connected to a laptop, which is programmed to record the reading every  $1 \text{ s}$ . The hydrogeophysical probes measure the soil water pressure and SP signals during the drainage

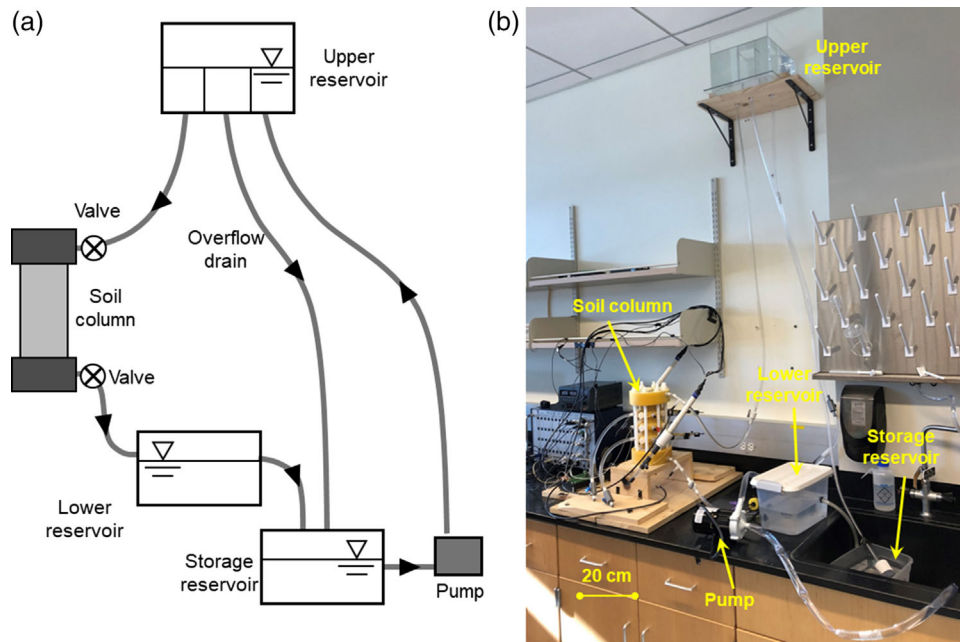


**FIGURE 4** The arrangement of the laboratory setup for saturated test: (a) a schematic and (b) the developed setup in this study. The water flow rate may be adjusted by partially opening the valve at the bottom of the soil column or by adjusting the position of the lower constant head reservoir relative to the soil column

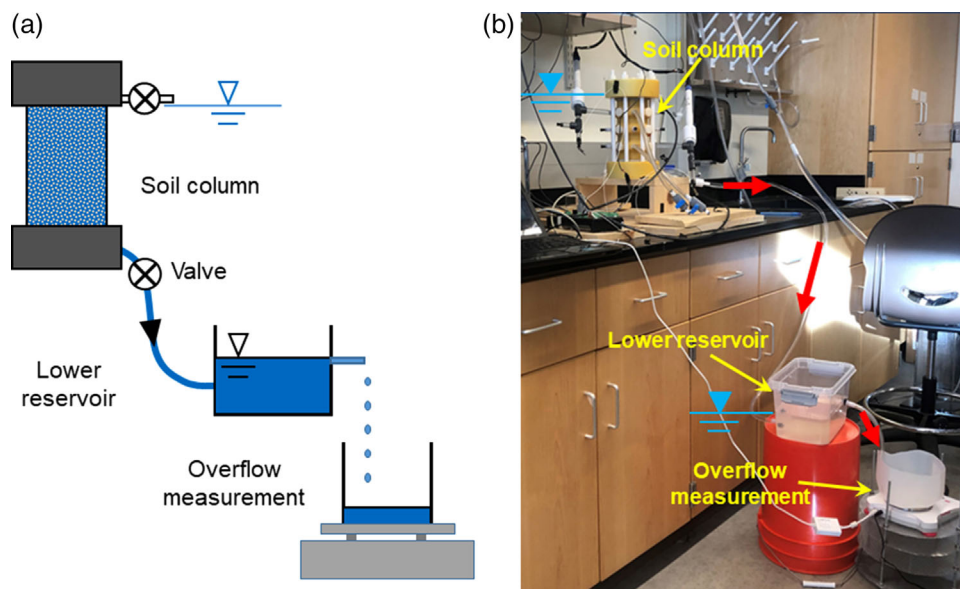


**FIGURE 5** The laboratory setup for the transient test: (a) the schematic and (b) the developed setup for this study. The valve at the top of the soil column is open, so the water in the soil sample is under atmospheric pressure. The valve at the bottom of the soil column is close before the transient test to keep the soil sample saturated

process. These transient data can be used to estimate the unsaturated hydraulic and electrical properties of the sample.

### 3 | EXPERIMENTAL PROCEDURES

In this section, we demonstrate the saturated flow and drainage test procedures using a reconstructed sand sample.

We also introduce the basic soil properties of the sand and the sample preparation. Using a sand sample is because the petrophysical properties of sand have been well studied, and many published datasets are available for comparison to validate our measurement. Undisturbed samples will not be considered for our test because the developed soil column has a rigid boundary. It is a challenge to trim an undisturbed soil sample to fit

**TABLE 1** Summary of the petrophysical properties of the sand sample

Soil properties	Value
Porosity, $\phi$ (–)	0.45
Saturated hydraulic conductivity ( $K_{\text{sat}}$ , $\text{m s}^{-1}$ )	$1.12 \times 10^{-3}$
Saturated streaming potential coupling coefficient ( $C_{\text{sat}}$ , $\text{V Pa}^{-1}$ )	$-7.19 \times 10^{-6}$
Dry density ( $\rho$ , $\text{g cm}^{-3}$ )	1.45
Real electrical conductivity at saturation <sup>a</sup> ( $\sigma'_{\text{sat}}$ , $\text{S m}^{-1}$ )	$8.9 \times 10^{-4}$
Imaginary electrical conductivity at saturation <sup>a</sup> ( $\sigma''_{\text{sat}}$ , $\text{S m}^{-1}$ )	$2.81 \times 10^{-5}$
Surface conductivity at saturation <sup>a</sup> ( $\sigma_s$ , $\text{S m}^{-1}$ )	$2.9 \times 10^{-4}$
Formation factor <sup>b</sup> ( $F$ )	3.31
Grain size at which 10% of the soil is finer by weight ( $d_{10}$ , mm)	0.2
Grain size at which 50% of the soil is finer by weight ( $d_{50}$ , mm)	0.5

<sup>a</sup>The measurement frequency is 0.01 Hz.

<sup>b</sup>Estimated using  $F = \phi^{-m}$  by assuming cementation exponent  $m = 1.5$ .

the rigid soil column perfectly. Note that any gap between the sample and the sidewall of the cell may create significant measurement biases.

### 3.1 | Basic soil properties

The tested sand sample is collected from a river bar next to Mores Creek near Boise, ID. The X-ray diffraction analysis indicates that the sample contains 13% quartz, 25% K-feldspar, 58% plagioclase, and 4% mica by weight. The grain size distribution of the sample is determined using sieving. The maximum grain size is  $\sim 2$  mm, and the smallest grain size is smaller than 0.053 mm. The grain size  $d_{10}$  (at which 10% of the soil is finer by weight) is 0.2 mm, and the grain size  $d_{50}$  (at which 50% of the soil is finer by weight) is 0.5 mm. These properties are summarized in Table 1.

### 3.2 | Sample preparation

The soil sample is prepared in the cylindrical cell by mechanical packing. Special care is taken to ensure the arrangement of grains is consistent throughout the soil sample because any heterogeneities can significantly influence the hydrologic properties (Allègre et al., 2014). To prepare the sample, we weigh 200 g of the dry sand sample at its residual moisture content and then place it in the cell. A porous stone is placed at the bottom of the cell, and it will prevent the grains from moving out of the inlet/outlet of the soil column during the flow test. The soil sample in the column is then tamped 30 times with a wooden tamp. This process is repeated until the soil sample reaches the height at which a hydrogeophysical probe needs to be inserted. At this point, the ceramic cup side of the probe is threaded into the soil column. During the preparation, the pressure transducer is not attached to the probe. The probe

is considered secure when the tip of the ceramic cup is about a millimeter from the cylinder wall. This installation ensures the ceramic cup has a sufficient contact area with the soil. After the hydrogeophysical probe is installed, adding soil to the cell can be resumed until the next hydrogeophysical probe needs to be installed. Once the cylindrical cell is full, another porous stone is placed on top of the sample. Afterward, the end cap may be put on with an O-ring and nuts tightened. If a leak occurs at the bottom or top of the soil column, and then press-to-seal rope caulking can be used to further seal the soil column.

Once the sand is packed in the soil column, the bulk density of the sample can then be determined based on the total mass used and the volume of the soil column. Next, the residual soil moisture content of the sand sample is measured, and then the dry density and porosity of the soil sample can be calculated. Assuming the grain density is  $2.65 \text{ g cm}^{-3}$ , a typical value for quartz and feldspar, we calculate the sample's porosity  $\phi = 45\%$ .

### 3.3 | Saturation

In this study, the soil sample prepared in the cylindrical cell is saturated with distilled water. We take the following steps to saturate the sample. First, we use a hose to connect the bottom of the soil column to the upper reservoir (Figure 4). Next, water is pumped from the storage reservoir to the upper reservoir until a constant head is reached. Once a constant head is reached, the valve at the bottom of the soil column is opened to start the saturation process. The flow rate is kept low such that the water level in the soil sample increases slowly, ensuring no air is trapped in the sample. During the saturation process, water will enter the hydrogeophysical probes via the porous ceramic cups. When the tube of probes is full of water and free of any air bubbles, the pressure transducer is attached. At

the top of the soil column, another hose is used to connect the inlet and an empty reservoir above the soil column. The upper valve remains open during the saturation process, and thus the air in the soil sample can leave the cell easily. From the transparent hose, we can visualize the water level and decide if the saturation is complete.

When the saturation is complete, the hoses are arranged so that water enters the soil column from the top and exits through the bottom, as shown in Figure 4. Although distilled water is used to saturate the soil sample, soil grains may have some chemical reactions with water, increasing the concentration of ions in the pore water (e.g., Leroy et al., 2008). To ensure a homogenous water conductivity, we cycle the water through the soil column until there is no significant change in  $\sigma_w$  within 10 min. A final check is then made to ensure the upper and lower reservoirs are filled with water with a constant head and no air bubbles in the hoses.

The water–mineral interaction can occur during an extended time (Leroy et al., 2008). Therefore, over time, the pore water chemistry in the soil sample may change and be different from the water in the hydrogeophysical probes. This chemical difference/gradient between the sample and probes could induce an SP signal with a diffusion nature, which will be a perturbation to the streaming potential (Jougnot & Linde, 2013). Therefore, in processing SP data, this possible measurement bias should be considered.

### 3.4 | Saturated test

Once the sample is saturated, the saturated flow and SP tests may begin by circulating water through the sample at constant flow rates. During the test, soil water pressure, temperature, and electrical potential will be measured with the two hydrogeophysical probes, and the data are recorded every 0.5 s. The saturated test begins with a hydrostatic period of at least 20 min. This hydrostatic period ensures no water moves in the soil column, and thus the initial electrical potential measured by the two probes can be recorded. Following the hydrostatic stage, five different hydraulic gradients are applied to the sample, each lasting 20 min. The hydraulic gradient may be adjusted by partially closing the valve at the bottom of the soil column or by moving the elevation of the lower reservoir. Water is collected for the final 10 min of each interval from the lower reservoir for flow rate determination. The water conductivity and pH of the sampled water are also measured. After completing the saturated flow tests, the bottom valve is closed to return the sample to a hydrostatic state for another 20 min. During this period, the pore water pressure, electrical potential, and temperature are also recorded.

After completing the saturated flow test, the saturated complex conductivity  $\sigma_{sat}^*$  of the sample can be measured. In the test, electrical current is injected into the soil sample through

the electrodes installed at the inlet and outlet of the soil column, and the induced electrical potential in the sample is measured with the two hydrogeophysical probes. In this study, the complex conductivity meter (PSIP, Ontash & Ermac, Inc.) is used to conduct the measurement, and the covered frequency ranges between 0.01 and 1 Hz. Based on the geometry of the sample and positions of the electrodes, the associated geometric factor can be determined, and thus the measured impedance can be converted into complex conductivity. The measured water conductivity  $\sigma_w$  of the sample in this study is  $1.99 \times 10^{-3} \text{ S m}^{-1}$ .

### 3.5 | Drainage test

Once the saturated test is complete, the experimental setup can be rearranged to perform the drainage test (Figure 5). Before testing, the hose connection between the upper reservoir and soil column is removed, but we keep the sample saturated by closing the bottom valve. Thus, the sample in the cell is in the hydrostatic condition, and the water level is on the soil surface (Figure 5). Additionally, the elevation of the lower reservoir is adjusted to be  $\sim 60$  cm below the bottom of the soil column. A water collection vessel is placed at the outlet of the lower reservoir, and a digital balance monitors its weight.

Before drainage begins, measurements are made while the sample is at the hydrostatic state, for example, for 5 min. The drainage process will begin once the bottom valve is opened. Due to gravity, the water in the sample will flow downward. For the tested sand sample, the drainage process will last several hours, during which the outflow mass (volume), pore water pressure, and electrical potential induced by unsaturated water flow are recorded. The complex conductivity measurement cannot be performed during the transient process because SP signals will be corrupted if an electrical current is injected into the sample.

## 4 | SATURATED TEST RESULTS

In this section, we report the saturated test results of the sand sample, including the saturated hydraulic conductivity  $K_{sat}$ , saturated streaming potential coupling coefficient  $C_{sat}$ , and saturated complex conductivity  $\sigma_{sat}^*$ .

### 4.1 | Saturated hydraulic conductivity $K_{sat}$

The soil pore water pressure measured by the two hydrogeophysical probes during the saturated flow test is shown in Figure 6, in which the water pressure is presented as total head  $h$ , that is, the sum of pressure head  $h_p$  and elevation head  $h_z$  (using the bottom of the soil column as the datum).

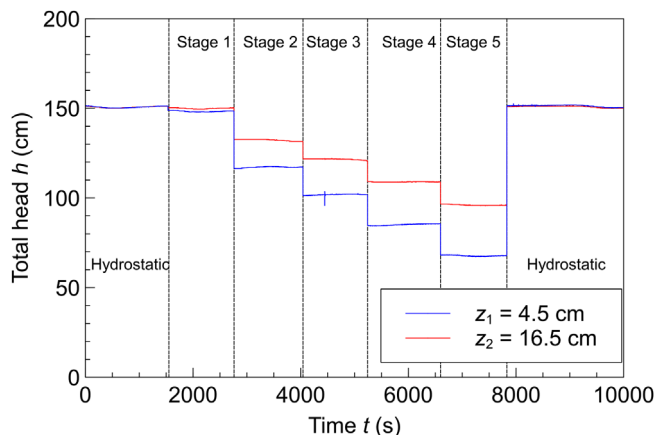


**FIGURE 6** Total water head measured at the two elevations ( $z_1 = 4.5$  cm and  $z_2 = 16.5$  cm) of the soil column during the saturated flow test. Dash lines indicate the boundary between two adjacent flow stages

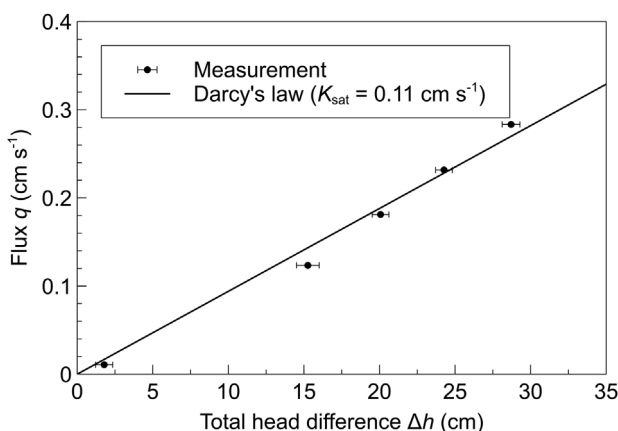


**FIGURE 7** Total head difference  $\Delta h$  and water flux  $q$  measured for the five stages of the saturated flow test. The measurement uncertainty of  $q$  is indicated by the error bar. The solid line represents Darcy's law with a saturated hydraulic conductivity  $K_{\text{sat}}$  of  $0.11$  cm  $\text{s}^{-1}$

As shown in the figure, the time series of  $h$  at the two elevations ( $z_1 = 4.5$  cm and  $z_2 = 16.5$  cm) show a clear stepwise response. Before  $\sim 1,700$  s, the sample is in the hydrostatic condition, and the total head at these two elevations is identical  $\sim 151$  cm. Once the water starts to flow through the sample,  $h$  at the two elevations decreases due to hydraulic losses in the sample. Five flow rates are achieved in our test (Figure 6). The measured total head  $h$  reaches a minimum value of  $\sim 67$  and  $\sim 95$  cm for the upper and lower elevations, respectively.

The total head difference  $\Delta h$  measured between the two probes for these five stages are determined as 1.6, 15.2, 19.8, 23.8, and 28.2 cm, and the measured water flux  $q$  is 0.011, 0.123, 0.181, 0.232, and 0.283 cm  $\text{s}^{-1}$ . These two datasets are cross-plotted in Figure 7, in which the measurement uncertainty (one standard deviation) of  $\Delta h$  is also indicated. The uncertainty of  $\Delta h$  is relatively small, generally lower than

1 cm, showing the excellent performance of the hydrogeophysical probes in measuring the positive soil water pressure (relative to atmospheric pressure). The water flux  $q$  and total head difference  $\Delta h$  show a nearly perfect linear relationship (Figure 7). Using Darcy's law, the saturated hydraulic conductivity  $K_{\text{sat}}$  can be calculated as  $9.66 \times 10^{-4}$  m  $\text{s}^{-1}$ . We also estimate the possible range of  $K_{\text{sat}}$  as the range bounded by the minimum and maximum  $K_{\text{sat}}$  calculated using data of individual stages. The calculated range of  $K_{\text{sat}}$  is between  $6.04 \times 10^{-4}$  and  $9.87 \times 10^{-4}$  m  $\text{s}^{-1}$  and is typical for coarse sands (Mitchell & Soga, 2005). Consider the Kozeny–Carman equation, expressed as (e.g., Mitchell & Soga, 2005)

$$K_{\text{sat}} = \frac{\mu}{\gamma} \frac{d^2}{36\tau^2 k_0} \frac{\phi^3}{(1-\phi)^2} \quad (1)$$

where  $\mu$  is the dynamic viscosity of water ( $8.9 \times 10^{-4}$  Pa  $\text{s}^{-1}$ ),  $\gamma$  is the unit weight of water ( $10^4$  N  $\text{m}^{-3}$ ),  $d$  is the characteristic grain size,  $\tau$  is the hydraulic tortuosity,  $k_0$  is a shape factor (e.g., equal to 2.5; see Mitchell and Soga [2005]). Using Equation 1, we can estimate the hydraulic conductivity of the sand sample as  $6.77 \times 10^{-4}$  m  $\text{s}^{-1}$ . In the prediction, we use  $d_{10} = 0.2$  mm as the characteristic grain size and use  $F\phi$  ( $F = \phi^{-1.5}$  being the formation factor) as the hydraulic tortuosity (e.g., Slater et al., 2014). The close match between measured and predicted  $K_{\text{sat}}$  and narrow variation range of  $K_{\text{sat}}$  show that the developed soil column system works well for determining the saturated hydraulic conductivity of the sample.

## 4.2 | Saturated streaming potential coupling coefficient $C_{\text{sat}}$

The electrical potential  $V$  measured by the two hydrogeophysical probes at  $z_1 = 4.5$  cm and  $z_2 = 16.5$  cm during the saturated flow test are shown in Figure 8. Both measurements use the negative terminal of the DC power of the data logger as the ground (reference). At first glance, it is obvious that both  $V$  signals in Figure 8 decrease during the test, although there are many spikes. It seems the variations in  $V$  are not associated with the changes in the water pressure measured during the flow test (Figure 7). Indeed, the variation in  $V$  observed in Figure 8 generally reflects the potential changes of grounding, that is, the potential at the negative terminal of the DC power of the data logger, which is significantly larger than the streaming potential. Thus, the water flow-induced electrical potential (i.e., streaming potential) is masked.

To eliminate the influence of grounding, we calculate the SP signal as the electrical potential difference  $\Delta V$  between the upper and bottom probes. Before calculating the difference, the 10th order moving average filter is applied to the  $V$  time series. It has been found that nonpolarizing electrodes may

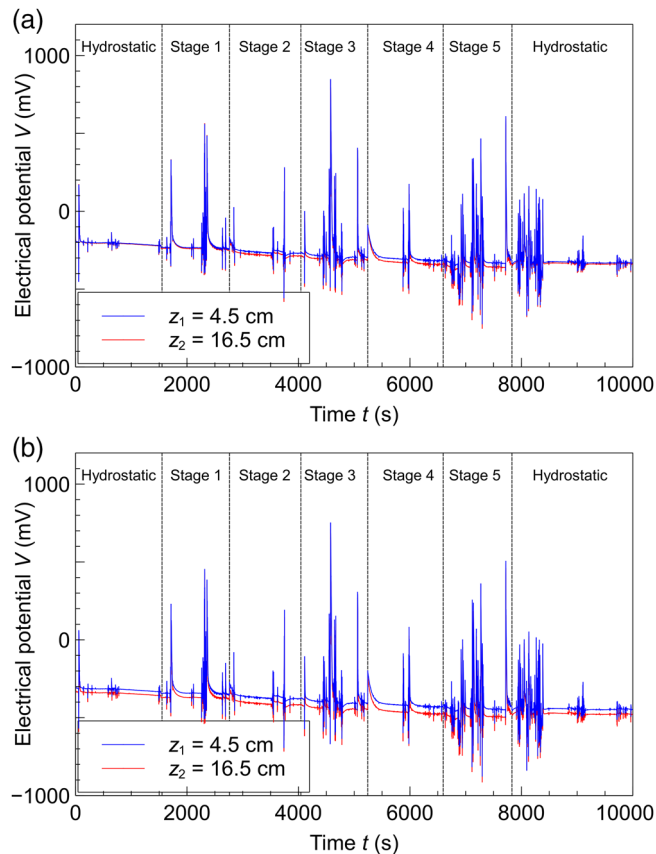


**FIGURE 8** Measured electrical potential during the saturated flow test: (a) hydrogeophysical probes and (b) traditional installation of Ag/AgCl electrodes. The negative terminal of the DC power of the data logger is used as the reference for the potential measurement. Dash lines indicate the boundary between two adjacent flow stages

drift due to the temperature fluctuation or ionic diffusion occurring between the probe and pore water (e.g., Jardani et al., 2009; Jougnot & Linde, 2013). To remove this effect, we process the  $\Delta V$  data with the following steps (similar to that used in Jardani et al., [2009]): (a) shift calculated potential difference curve such that the  $\Delta V$  value at the initial hydrostatic stage is zero; (b) determine the residual potential difference at the second hydrostatic stage  $\Delta V_r$ ; (c) assume  $\Delta V_r$  was developed linearly with time between the two hydrostatic stages; and (d) subtract this time-dependent  $\Delta V_r$  from the shifted potential difference curve. The resulted potential difference curves are shown in Figure 9a for both the hydrogeophysical probes and the traditional Ag/AgCl electrodes.

In Figure 9a, the boundary between two adjacent flow stages can be easily identified now. It appears that the SP signal ( $\Delta V$ ) during each stage does not stay a perfect constant. In particular, the variations in Stages 3 and 4 are quite large, reaching up to  $\sim 35\%$  of the average value of each stage. To evaluate if this variation is from the temperature effect, we also monitored the water temperature within the upper hydrogeophysical probe, and the results are shown in Figure 9b. A

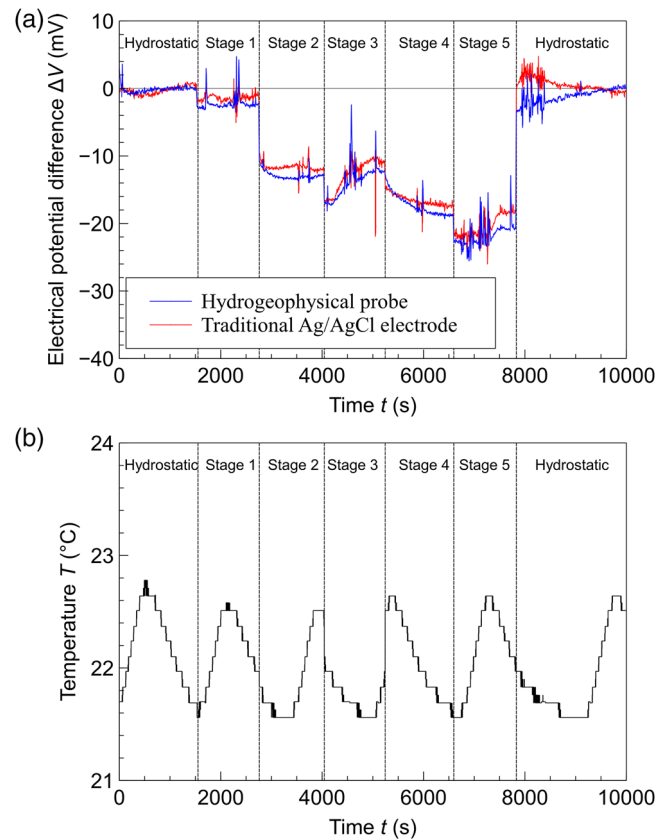


**FIGURE 9** The experimental results of the saturated flow test: (a) self-potential (SP) data and (b) water temperature with the upper hydrogeophysical probe. The SP is presented as the electrical potential difference  $\Delta V$  between the upper and lower hydrogeophysical probes (or traditional Ag/AgCl electrodes) after removing drifting (see main text). Dash lines indicate the boundary between two adjacent flow stages

variation of  $\sim 1.3^\circ\text{C}$  is observed. Considering a mean room temperature of  $22^\circ\text{C}$  and a Cl<sup>-</sup> activity of  $10^{-4}$ , a temperature fluctuation of  $1.3^\circ\text{C}$  could induce a disturbance of  $\sim 0.97\text{ mV}$  for Ag/AgCl electrodes (see Equation 7 in Jougnot and Linde [2013]). Compared with the SP values recorded in our experiment (typically larger than 10s of mV; see Figure 9a), the effect of the temperature is marginal. In particular, the two hydrogeophysical probes are outside of the soil column, and water temperature within both probes is likely to vary with the room temperature. Considering both probes have the same design and materials, the temperature difference between the two probes should be minor. Accordingly, the effect of temperature fluctuation on the potential difference  $\Delta V$  should be even smaller than  $0.98\text{ mV}$ . Indeed, during the first hydrostatic stage, the streaming potential is zero because of no water flow. Although the temperature varies between  $21.5$  and  $22.8^\circ\text{C}$  (Figure 9b), the  $\Delta V$  calculated from the two hydrogeophysical probes is still almost constant with a standard deviation of  $\sim 0.5\text{ mV}$ . Thus, it is safe to conclude that the effect of temperature on the calculated  $\Delta V$  in Figure 9a is marginal.

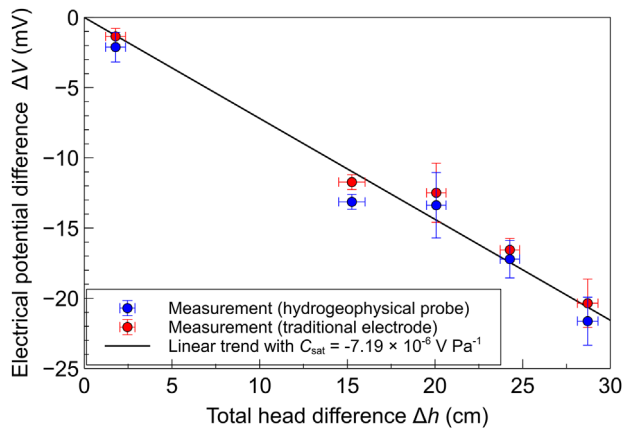


**FIGURE 10** Average electrical potential difference  $\Delta V$  and total head difference  $\Delta h$  of different stages of the saturated flow test. The uncertainties (standard deviation) of  $\Delta V$  and  $\Delta h$  are indicated by the error bars. The solid line represents a linear fitting to the hydrogeophysical probe data with a saturated streaming potential coupling coefficient  $C_{\text{sat}}$  of  $-7.2 \times 10^{-6} \text{ V Pa}^{-1}$

To determine  $C_{\text{sat}}$ , we calculate each stage's average SP value ( $\Delta V$ ) and plot them in Figure 10 against  $\Delta h$ . We also use the standard deviation of  $\Delta V$  in each stage to quantify the uncertainty of SP measurement, and they are indicated by the vertical error bar in Figure 10. Although it seems the SP signals in Figure 9 show large variations, the uncertainty in each stage is still marginal compared with the mean value (Figure 10). The average  $\Delta V$  and  $\Delta h$  show a nearly perfect linear relationship, typical for sand samples (e.g., Guichet et al., 2006). Using linear fitting, we determine  $C_{\text{sat}}$  as  $-7.2 \times 10^{-6} \text{ V Pa}^{-1}$ . The maximum and minimum  $C_{\text{sat}}$  are calculated using the same method as  $K_{\text{sat}}$ , and the determined variation range of  $C_{\text{sat}}$  is between  $-12.1 \times 10^{-6} \text{ V Pa}^{-1}$  and  $-6.8 \times 10^{-6} \text{ V Pa}^{-1}$ . Previous studies show that the grain size has a dominating effect on  $C_{\text{sat}}$  of granular soils (e.g., Glover & Déry, 2010). For glass beads with similar grain size  $d$  (ranging between 0.048 and 0.99 mm) and water conductivity ( $\sigma_w = 2.44 \times 10^{-3} \text{ S m}^{-1}$ ), Glover and Déry (2010) reported that the measured  $C_{\text{sat}}$  is between  $-23.2$  and  $-13.7 \times 10^{-6} \text{ V Pa}^{-1}$ . In general, the glass beads samples show a relatively higher coupling coefficient, about two times higher. However, considering the difference in mineralogy and  $\sigma_w$ , the two  $C_{\text{sat}}$  measurements are still in reasonable agreement.

### 4.3 | Saturated complex electrical conductivity $\sigma_{\text{sat}}^*$

The complex electrical conductivity of the saturated sand sample is also measured in the frequency range between 0.01 and 1 Hz. We do not observe a significant change in the real conductivity  $\sigma'_{\text{sat}}$  and imaginary conductivity  $\sigma''_{\text{sat}}$  in this frequency range (see Figure 11), and thus we only discuss the

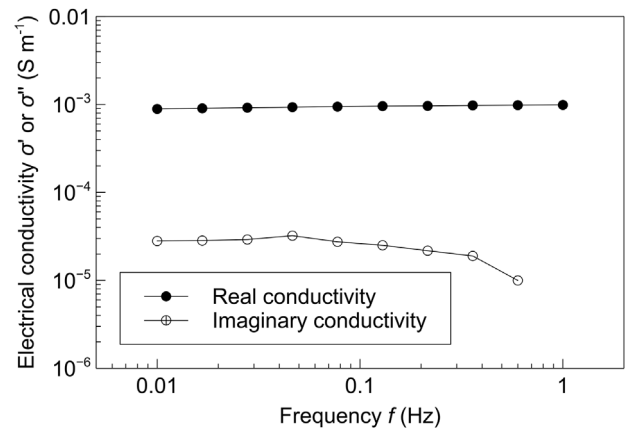


**FIGURE 11** Complex conductivity of the saturated sand sample measured in the frequency range between 0.01 and 1 Hz

measurements at 0.01 Hz here. The measured  $\sigma'_{\text{sat}}$  and  $\sigma''_{\text{sat}}$  of the sample at 0.01 Hz are  $8.9 \times 10^{-4} \text{ S m}^{-1}$  and  $2.81 \times 10^{-5} \text{ S m}^{-1}$ , respectively. If we assume the cementation factor  $m$  of the sample is 1.5, a typical value for sand (Friedman, 2005), the formation factor  $F$  can be estimated using Archie's law (Archie, 1942) as  $\phi^{-m} = 3.29$ . Then, the surface conductivity  $\sigma_s$  of the sample at saturation can be determined as  $\sigma_s = \sigma'_{\text{sat}} - \sigma_w/F$  as  $2.85 \times 10^{-4} \text{ S m}^{-1}$ , which is significant compared with the contribution from bulk water ( $6.05 \times 10^{-4} \text{ S m}^{-1}$ ). The relatively significant contribution of surface conduction is due to the low water salinity used in the test (Revil et al., 2014). Using a higher  $m$  value ( $m = 2$ ), we can calculate  $F = 4.89$ , and  $\sigma_s$  can be calculated as  $4.83 \times 10^{-4} \text{ S m}^{-1}$ . Thus, we estimate the surface conductivity of the sand sample in our study is between  $2.85$  and  $4.83 \times 10^{-4} \text{ S m}^{-1}$ . Using  $d_{50}$  (0.5 mm) as the effective grain size  $d_{\text{eff}}$ , the sample's specific surface conductance  $\Sigma_s = \sigma_s d_{\text{eff}}/4$  (e.g., Leroy et al., 2008) is calculated between  $3.6$  and  $6.0 \times 10^{-8} \text{ S}$ . Note that for natural sands and sandstones, Revil and Glover (1998) calculated the specific surface conductance  $\Sigma_s$  as  $\sim 5 \times 10^{-9} \text{ S}$  at similar water salinities (e.g.,  $\sim 10^{-4} \text{ mol L}^{-1}$ ) using their surface conductivity theory. For the sample tested in this study, it seems the specific surface conductance is about one order higher, indicating feldspar-rich samples may have different surface chemistry from quartz- and clay-rich soils. More investigations, however, are required to explain this observation.

## 5 | DRAINAGE TEST RESULTS

In this section, we report the transient responses of the sand sample during the drainage test, including cumulative outflow volume  $Q$ , pore water pressure head  $h_p$ , and electrical potential  $V$ . Estimations of soil parameters governing saturated/unsaturated flows are also performed using the measured transient responses.

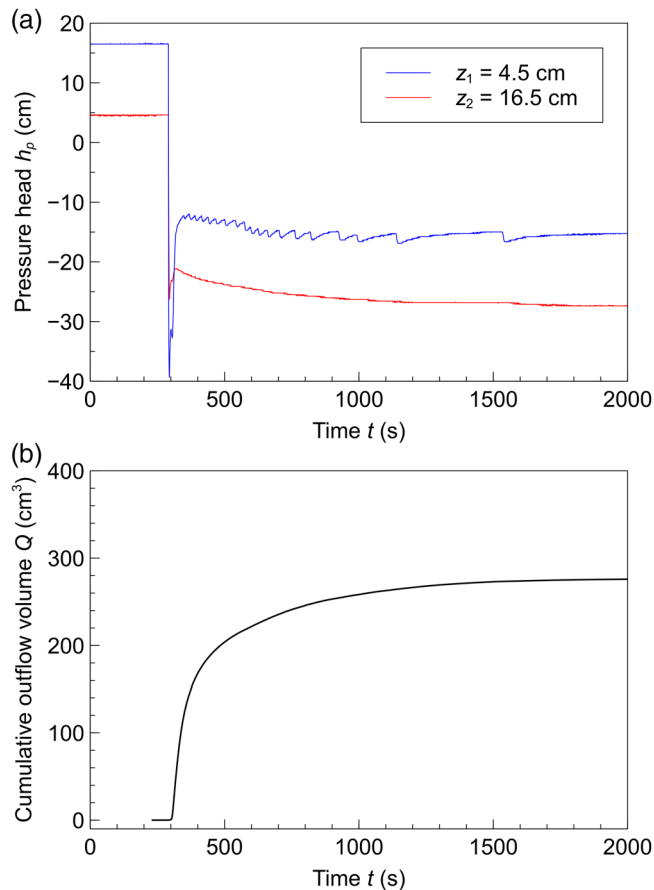


**FIGURE 12** Hydraulic responses of the sand sample during the drainage test: (a) pore water pressure head measured at two elevations  $z_1$  and  $z_2$  and (b) cumulative outflow volume  $Q$

## 5.1 | Transient responses

The drainage test lasts  $\sim 30$  min, during which the pore water pressure head  $h_p$  and electrical potential  $V$  are measured by two hydrogeophysical probes. The outflow is collected at the lower reservoir and monitored by the digital scale. The hydraulic responses ( $Q$  and  $h_p$ ) are shown in Figure 12. It is clear that before the drainage is initiated at  $t = 290.5$  s, both probes measure their respective hydrostatic pressures. Once the outflow starts, the pressure head  $h_p$  at both elevations drops drastically within a very short time ( $\sim 5$  s), reaching their minimal values. For instance,  $h_p$  at elevation  $z_1 = 4.5$  cm drops from its initial value 16.5 cm to about  $-39.4$  cm; at elevation  $z_2 = 16.5$  cm,  $h_p$  decreases from 4.5 cm to about  $-26.3$  cm. During this short period ( $\sim 5$  s), little cumulative outflow ( $<0.2$  cm<sup>3</sup> water) is observed, indicating that the pore water pressure responds quickly to the applied boundary condition  $h_b = -60$  cm.

After reaching a minimum value, the water pressure at both locations starts to increase. About 30 s after applying  $h_b$ , the pressure head  $h_p$  increases to a peak,  $-12.4$  cm at  $z_1 = 4.5$  cm and  $-21.1$  cm at  $z_2 = 16.5$  cm. The increase in  $h_p$  is because

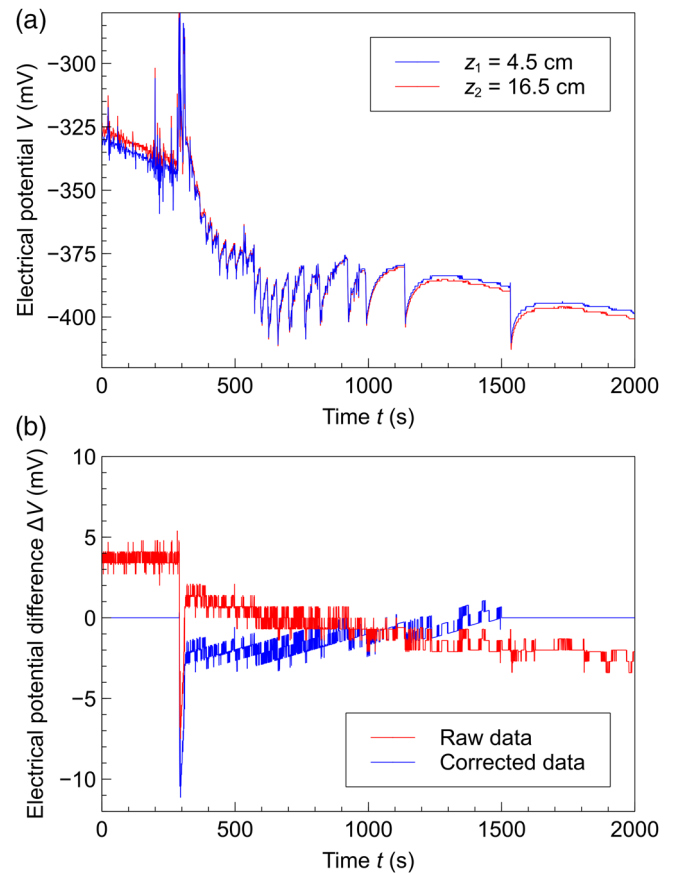


**FIGURE 13** Self-potential (SP) responses of the sand sample during the drainage test: (a) electrical potential  $V$  measured at two different elevations  $z_1$  and  $z_2$  and (b) electrical potential difference  $\Delta V$  measured between the top and bottom probes. In (b), the red line represents  $\Delta V$  calculated directly from  $V$  measurement, and the blue line is  $\Delta V$  after correction (see main text for details)

water from higher elevations has moved downward to balance the pressure drops induced by applying  $h_b$ . In the next stage ( $t > 350$  s), the water pressure at both elevations gradually decreases towards a constant pressure. At  $t = 2,000$  s, the water pressure head is  $-27.4$  cm at  $z_1 = 16.5$  cm and  $-15.3$  cm at  $z_2 = 4.5$  cm. The measured pressure head difference between these two probes is  $\sim 12.1$  cm, roughly equal to their elevation difference (12 cm). This means  $h_p$  at these two locations has reached equilibrium, and no significant water flow should occur. The cumulative outflow data in Figure 12b confirm that no significant increase in  $Q$  is observed at  $t = 2,000$  s.

The electrical potential  $V$  measured by the two probes during the drainage test is shown in Figure 13a. Note that the reference of the electrical potential measurement is the negative terminal of the power of the data logger. As shown in Figure 13a, the measured  $V$  of the two probes shows a similar trend. In general,  $V$  decreases from its initial value about  $-330$  mV at  $t = 0$  s to about  $-400$  mV at  $t = 2,000$  s. Even in the hydrostatic stage ( $t < 290$  s) or when the overflow

**TABLE 2** Summary of the prior knowledge of soil parameters and the estimated parameters from hydrogeophysical inversion of transient responses of the sand sample. The soil parameters include saturated water content  $\theta_s$ , residual water content  $\theta_r$ , parameter  $\alpha$  characterizing the air entry value, parameter  $n$  defining the shape of water retention curve, the logarithm of the saturated hydraulic conductivity  $\log K_{\text{sat}}$ , saturation exponent  $n_a$  in Archie's law, and the negative logarithm of the saturated streaming potential coupling coefficient  $-\log C_{\text{sat}}$

Soil parameters	Prior knowledge			Inversion results	
	Mean	Variance	Variation range	Mean	95% CI
$\theta_s, \text{m}^3 \text{m}^{-3}$	0.40	$0.04^2$	0.35 ~ 0.55	0.46	[0.40, 0.50]
$\theta_r, \text{m}^3 \text{m}^{-3}$	0.03	$0.012^2$	0 ~ 0.06	0.034	[0.004, 0.057]
$A, \text{m}^{-1}$	7.0	$1.4^2$	3 ~ 10	9.23	[7.89, 9.94]
$n (-)$	4.0	$1.5^2$	1.01 ~ 10	2.30	[1.98, 2.80]
$\log K_{\text{sat}}, \text{m s}^{-1\text{a}}$	-4.0	$0.6^2$	-5 ~ -2	-2.98	[-3.10, -2.84]
$n_a (-)$	2.5	$0.4^2$	1.5 ~ 3.5	1.82	[1.53, 2.24]
$-\log C_{\text{sat}}, \text{V Pa}^{-1\text{b}}$	6.0	$0.8^2$	3 ~ 7	4.97	[4.87, 5.07]

<sup>a</sup>The unit is for  $K_{\text{sat}}$ .

<sup>b</sup>The unit is for  $C_{\text{sat}}$ .

nearly ceases ( $t > 1,500$  s), the measured electrical potential still varies with time. To remove the effects of common environmental factors (e.g., temperature and grounding) on the potential measurement, we calculate the electrical potential difference  $\Delta V$  between the upper and lower hydrogeophysical probes. The results are plotted in Figure 13b (red line). As shown in the figure,  $\Delta V$  stays almost constant before the flow starts ( $< 300$  s) and after the outflow is ceased ( $> 1,500$  s). This constant  $\Delta V$  implies that the large potential variations recorded in individual electrodes (Figure 13a) are mainly from environmental factors such as temperature and grounding/reference.

It is apparent that the calculated  $\Delta V$  is associated with the drainage process. In the hydrostatic stage ( $t < 290.5$  s),  $\Delta V$  is nearly constant ( $\sim 4$  mV); after the drainage starts at  $t = 290.5$  s, there is a sharp decrease in  $\Delta V$ , which corresponds to the quick increase in the overflow (Figure 12b). The lowest potential difference reaches  $\sim -7$  mV, about 11 mV smaller than the value in hydrostatic conditions. About 50 s after the onset of the drainage,  $\Delta V$  increases to  $\sim 1$  mV from the minimum value ( $-7$  mV); at this point, the overflow has been significantly small. Between  $t = \sim 350$  s and  $t = 1,500$  s, both  $Q$  and  $\Delta V$  change gradually with time. After  $t = 1,500$  s, the increase in  $Q$  is rather small, and accordingly, no significant change in SP (i.e.,  $\Delta V$ ) is observed, as shown in Figure 13b.

In principle, when  $Q$  is not increasing significantly (e.g.,  $t > 1,500$  s), the measured  $\Delta V$  should go back to its initial value ( $\sim 4$  mV) in hydrostatic condition (i.e.,  $t < 290.5$  s). This is because, at both stages, not water flux exists in the soil sample, and thus the streaming potential should be zero. However, we observe a small offset ( $\sim 2$  mV) in  $\Delta V$  between these two stages. A similar  $\Delta V$  response has been reported in Allègre et al. (2014). The offset is less likely from the electrode drifting because  $\Delta V$  stays constant for  $t < 290.5$  s and  $t > 1,500$  s. The drainage-induced water content decrease and thus electrical resistivity increase of the sample might be responsible for

the observed  $\Delta V$  offset. In this study, we assume the  $\Delta V$  offset increases linearly from zero at  $t = 290.5$  s to 2 mV at  $t = 1,500$  s. The measured  $\Delta V$  (red line in Figure 13b) is thus corrected by removing this offset. We also shift the curve downward to make  $\Delta V$  in the hydrostatic condition as zero. The corrected  $\Delta V$  is plotted in Figure 13b (blue line), and it will be used in the following to estimate the unsaturated soil properties. It should be addressed that the corrected  $\Delta V$  response is similar to the simulated SP signal of the synthetic sand during drainage, as reported in Xie et al. (2021).

## 5.2 | Coupled, stochastic hydrogeophysical inversion

The transient responses of the sand during drainage ( $Q$ ,  $h_p$ , and  $\Delta V$ ) are used to estimate the saturated/unsaturated properties of the sample using the coupled, stochastic hydrogeophysical inversion code developed in Xie et al. (2021). The inversion uses Markov Chain Monte Carlo (MCMC) technique to generate samples that follow the posterior distributions of the model parameters (Vrugt et al., 2003). In the inversion, the soil water retention curve (SWRC) of the soil is modeled with the van Genuchten equation (van Genuchten, 1980); the hydraulic conductivity function  $K$  is a Mualem type model (Mualem, 1976) based on the van Genuchten SWRC equation (e.g., Schaap & Leij, 2000). The associated model parameters include saturated water content  $\theta_s$ , residual water content  $\theta_r$ , parameter  $\alpha$  characterizing the air entry value, parameter  $n$  defining the shape of SWRC, and  $K_{\text{sat}}$ . The (real) electrical conductivity of unsaturated soil  $\sigma'$  is modeled with the modified Archie's law (e.g., Lesmes & Friedman, 2005),

$$\sigma' = \frac{\sigma_w}{F} S^{n_a} + \sigma_s \quad (2)$$

where  $n_a$  is the saturation exponent, and  $S = \theta/\phi$  is the degree of saturation. For the streaming potential coupling coefficient

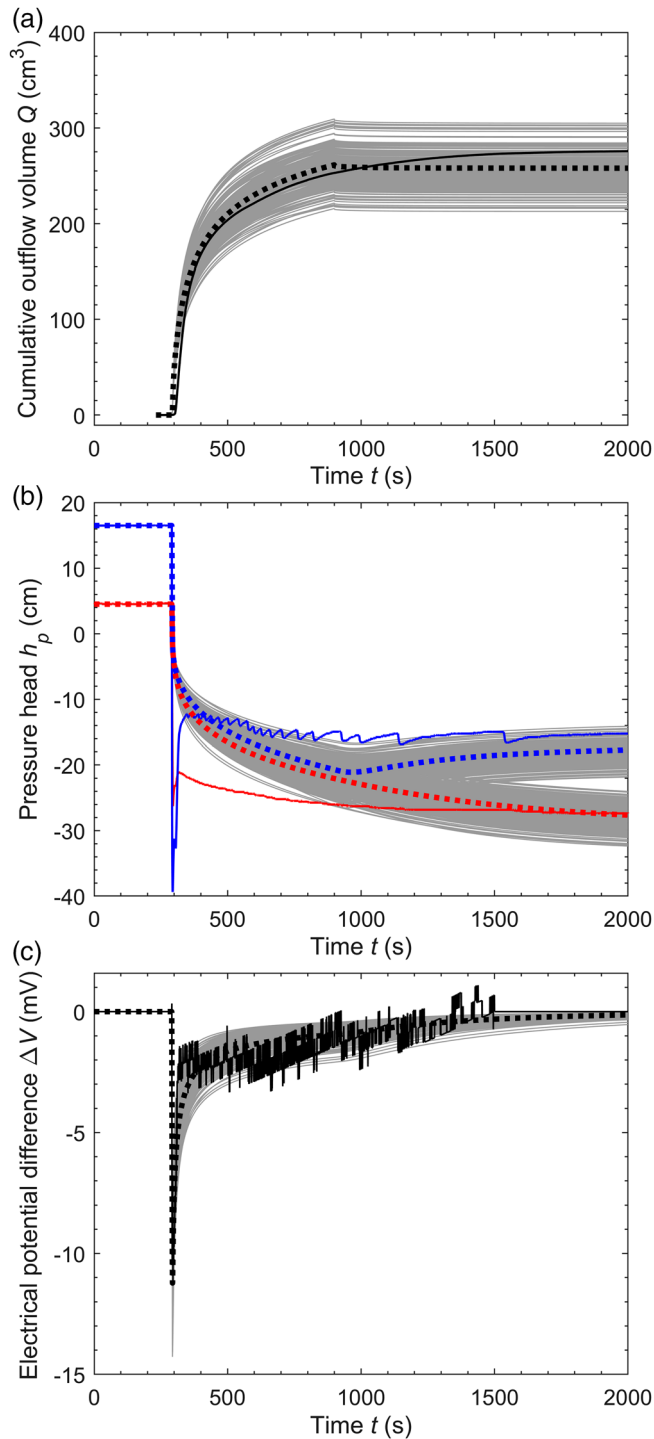


**FIGURE 14** The measured (solid line) and simulated average (dash line) transient responses of the sand sample during the drainage test: (a) the cumulative overflow volume  $Q$ , (b) the pressure head  $h_p$  at two elevations (blue line for  $z_1 = 4.5$  cm and red line for  $z_2 = 16.5$  cm); and (c) the electrical potential difference  $\Delta V$ . The shaded area represents the simulated responses using the random parameters generated from the 95% confidence intervals in Table 2

of unsaturated soils  $C$ , we use the following equation in the inversion (e.g., Linde et al., 2007),

$$C = \frac{C_{\text{sat}}}{S} \frac{K}{K_{\text{sat}}} \frac{\sigma'_{\text{sat}}}{\sigma'} \quad (3)$$

It is noted that other constitutive models may also be used in the inversion if necessary. Thus, the parameters to be recovered in the inversion include  $K_{\text{sat}}$ ,  $C_{\text{sat}}$ ,  $\theta_s$ ,  $\theta_r$ ,  $\alpha$ ,  $n$ , and  $n_a$ . In addition, other soil parameters such as  $\sigma_{\text{sat}}$ ,  $\sigma_w$ , and  $\sigma_s$  are assumed known and are assigned with the measured values from the saturated flow test.

For the stochastic inversion, the MCMC sampling is terminated after 30,000 runs in this study, and the first 20,000 runs are considered as the burn-in period, during which the covariances are not updated. The model parameters from the last 10,000 runs are used to estimate the statistical measures of the posterior distributions. Our prior knowledge of the mean, variances, and ranges of the model parameters can be determined empirically based on published data, and the values used in this study are summarized in Table 2.

### 5.3 | Estimated soil parameters

The inversion results, that is, the mean values and the 95% confidence intervals (CIs) of model parameters, are summarized in Table 2. The parameters  $K_{\text{sat}}$ ,  $C_{\text{sat}}$ , and  $\theta_s$  have been independently measured in the saturated test (Table 1), and thus we can compare them to the values estimated from hydrogeophysical inversion. The inverted  $\theta_s$  is 0.46, which is slightly higher than the porosity of the sand 0.45 (Table 1). The estimated mean value of  $K_{\text{sat}}$  from the drainage test is  $1.05 \times 10^{-3} \text{ m s}^{-1}$  ( $10^{-2.98} \text{ m s}^{-1}$ ), slightly larger than the direct measurement  $K_{\text{sat}} = 9.66 \times 10^{-4} \text{ m s}^{-1}$  with a relative difference of 8.7%; the variation ranges of  $K_{\text{sat}}$  determined from these two methods are quite similar,  $7.9 \times 10^{-4} \sim 1.44 \times 10^{-3} \text{ m s}^{-1}$  for the drainage test and  $6.04 \times 10^{-4} \sim 9.87 \times 10^{-3} \text{ m s}^{-1}$  for the saturated test. The estimated  $C_{\text{sat}}$  from the drainage test has a mean value of  $-10.7 \times 10^{-6} \text{ V Pa}^{-1}$  and a 95% CI of  $[-13.5 \times 10^{-6}, -8.5 \times 10^{-6}]$ , very close to the mean value  $-7.2 \times 10^{-6} \text{ V Pa}^{-1}$  and variation range  $(-12.1 \times 10^{-6} \sim -6.8 \times 10^{-6})$  determined from the saturated test. The close matches between direct measurement and inversion-based estimation of  $K_{\text{sat}}$ ,  $C_{\text{sat}}$ , and  $\theta_s$  prove that the coupled, stochastic hydrogeophysical inversion can extract the key electrical and hydraulic parameters of soils from transient responses collected during a drainage test.

Other estimated soil parameters are also typical values of sand samples. The inverse of the air-entry value parameter  $\alpha$  is  $9.23 \text{ m}^{-1}$ , which is very close to the measured value ( $1.3 \text{ kPa}^{-1}$  or  $13 \text{ m}^{-1}$ ) of glass beads with similar grain size ( $d_{50} = 0.6 \text{ mm}$ ) reported in Cao et al. (2018). The estimated  $n$

for the sand sample is 2.3; although it is lower than the measured  $n$  of glass beads (3.26) with similar grain size (Cao et al., 2018), it is still within the typical range (1.32~3.77) of sand samples (Schaap & Leij, 2000). The estimated mean value of the saturation exponent  $n_a$  is 1.82 for the sand sample, which is within the range (1.3~2) observed for unconsolidated sands (e.g., Schön, 1996).

Among all the parameters,  $K_{\text{sat}}$  has the lowest uncertainty with a relative length of the 95% CI (length of the 95% CI normalized by the mean value) of 8.7%, and  $\theta$ , has the highest uncertainty with a relative length of the 95% CI of 155.9%. The uncertainty of other parameters is generally small, lower than 40%. Using soil parameters randomly generated from the 95% CIs in Table 2, we calculate ~1,000 transient responses of the sand sample during the drainage test, and they are plotted in Figure 14 with gray lines. The transient responses calculated using the mean values are indicated with dash lines. Despite some local discrepancies, the simulated average  $Q$ ,  $h_p$ , and SP responses are generally matching the measurement, and the measured responses are within the variation range of the simulated responses.

While the agreement between measured and simulated  $Q$  and SP is excellent, the pressure head curves show large discrepancies. This could be due to the different boundary conditions applied to the bottom of the sand column in the test and simulation. While in the simulation, the pressure head boundary condition ( $h_b = -0.6$  m) is applied gradually to the soil column within a 5 s period,  $h_b$  in the experiment is applied suddenly. Thus, the measured  $h_p$  at two different elevations drops sharply following the onset of overflow. In addition, it is unclear how long this potential boundary condition ( $h_b = -0.6$  m) is maintained in the experiment. A small air bubble in the outlet of the soil column may change the boundary condition considerably. In the simulation, we simply remove this boundary condition ( $h_b = -0.6$  m) at  $t = 900$  s. Despite the local deviations, the general trends of  $Q$ ,  $h_p$ , and SP are in good agreement between the experiment and simulation, which justifies the recovered soil parameters (Table 2).

## 6 | CONCLUSIONS

In this study, we develop an integrated soil column system that measures both the electrical and hydraulic properties of soil samples. The soil column uses a novel hydrogeophysical probe that can effectively measure pore water pressure and electrical potential in soils in saturated flow and drainage tests. The saturated flow test can be used to directly measure the saturated hydraulic conductivity  $K_{\text{sat}}$ , saturated complex electrical conductivity  $\sigma_{\text{sat}}^*$ , and saturated streaming potential coupling coefficient  $C_{\text{sat}}$ . The drainage test can produce transient responses of pore water pressure, outflow, and SP, which

can be processed to estimate soil's key hydraulic and electrical properties. The soil column system requires only one sample to perform both saturated flow and drainage tests.

The experiment of a sand sample show that the developed soil column system is easy to operate. In addition, the determined saturated properties of the sand such as  $K_{\text{sat}}$ ,  $C_{\text{sat}}$ ,  $\sigma'_{\text{sat}}$ , and  $\sigma''_{\text{sat}}$  are within the typical ranges of sands reported in the literature. The unsaturated and saturated soil properties determined from coupled, stochastic hydrogeophysical inversion can well reproduce the measured transient responses of the sand sample during the drainage test. Moreover, the inversion-estimated saturated properties ( $\theta_s$ ,  $K_{\text{sat}}$ , and  $C_{\text{sat}}$ ) are very close to the values independently measured from the saturated test, proving the robustness of the developed system.

This new soil column system, including the novel hydrogeophysical probe, may be used to study regolith's hydraulic and electrical properties, which are vital in interpreting geophysical measurements in CZ hydrological studies. However, due to the complexity of CZ materials, there are several limitations of the developed setup. First, the current design only considers reconstituted samples. As is well known, the material structure may strongly affect the hydraulic and electrical properties of geological materials. Thus, the properties measured from reconstituted samples should be used with caution for geophysical field data interpretation. Second, some CZ materials have a fair amount of fine grains, and the associated experiments will take longer than the demonstrated sand sample. Thus, it is necessary to evaluate if the setup still works for clay- or silt-rich materials. Nevertheless, the developed setup constitutes a step forward in studying the petrophysical properties of CZ materials.

## ACKNOWLEDGMENTS

Acknowledgment is made to the Donors of the American Chemical Society Petroleum Research Fund for partial support of this research. Authors thank editor Prof. Sarah Garré for handling our submission, and two anonymous reviewers for their constructive comments, which have improved the quality of a previous version of the manuscript.

## AUTHOR CONTRIBUTIONS

Taylor Bienvenue: Data curation; Formal analysis; Investigation; Validation; Writing – original draft; Writing – review & editing. Jing Xie: Data curation; Formal analysis; Software; Validation; Visualization; Writing – review & editing. Qifei Niu: Conceptualization; Formal analysis; Funding acquisition; Methodology; Project administration; Resources; Supervision; Validation; Writing – review & editing.

## CONFLICT OF INTEREST

The authors declare no conflict of interest.

## ORCID

Qifei Niu  <https://orcid.org/0000-0003-2267-6653>

## REFERENCES

- Allègre, V., Jouniaux, L., Lehmann, F., & Sailhac, P. (2010). Streaming potential dependence on water-content in Fontainebleau sand. *Geophysical Journal International*, 182(3), 1248–1266. <https://doi.org/10.1111/j.1365-246X.2010.04716.x>
- Allègre, V., Maineuil, A., Lehmann, F., Lopes, F., & Zamora, M. (2014). Self-potential response to drainage–imbibition cycles. *Geophysical Journal International*, 197(3), 1410–1424. <https://doi.org/10.1093/gji/ggu055>
- Archie, G. E. (1942). The electrical resistivity log as an aid in determining some reservoir characteristics. *Transactions of the AIME*, 146(01), 54–62. <https://doi.org/10.2118/942054-G>
- Attwa, M., & Günther, T. (2013). Spectral induced polarization measurements for predicting the hydraulic conductivity in sandy aquifers. *Hydrology and Earth System Sciences*, 17(10), 4079–4094. <https://doi.org/10.5194/hess-17-4079-2013>
- Binley, A., Hubbard, S. S., Huisman, J. A., Revil, A., Robinson, D. A., Singha, K., & Slater, L. D. (2015). The emergence of hydrogeophysics for improved understanding of subsurface processes over multiple scales. *Water Resources Research*, 51(6), 3837–3866. <https://doi.org/10.1002/2015WR017016>
- Blanchy, G., Watts, C. W., Richards, J., Bussell, J., Huntenburg, K., Sparkes, D. L., Stalham, M., Hawkesford, M. J., Whalley, W. R., & Binley, A. (2020). Time-lapse geophysical assessment of agricultural practices on soil moisture dynamics. *Vadose Zone Journal*, 19(1), e20080. <https://doi.org/10.1002/vzj2.20080>
- Breede, K., Kemna, A., Esser, O., Zimmermann, E., Vereecken, H., & Huisman, J. A. (2011). Joint Measurement Setup for Determining Spectral Induced Polarization and Soil Hydraulic Properties. *Vadose Zone Journal*, 10(2), 716–726. <https://doi.org/10.2136/vzj2010.0110>
- Breede, K., Kemna, A., Esser, O., Zimmermann, E., Vereecken, H., & Huisman, J. A. (2012). Spectral induced polarization measurements on variably saturated sand-clay mixtures. *Near Surface Geophysics*, 10(6), 479–489. <https://doi.org/10.3997/1873-0604.2012048>
- Brooks, P. D., Chorover, J., Fan, Y., Godsey, S. E., Maxwell, R. M., McNamara, J. P., & Tague, C. (2015). Hydrological partitioning in the critical zone: Recent advances and opportunities for developing transferable understanding of water cycle dynamics. *Water Resources Research*, 51(9), 6973–6987. <https://doi.org/10.1002/2015WR017039>
- Cao, J., Jung, J., Song, X., & Bate, B. (2018). On the soil water characteristic curves of poorly graded granular materials in aqueous polymer solutions. *Acta Geotechnica*, 13(1), 103–116. <https://doi.org/10.1007/s11440-017-0568-7>
- Doussan, C., & Ruy, S. (2009). Prediction of unsaturated soil hydraulic conductivity with electrical conductivity. *Water Resources Research*, 45(10). <https://doi.org/10.1029/2008WR007309>
- Friedman, S. P. (2005). Soil properties influencing apparent electrical conductivity: A review. *Computers and Electronics in Agriculture*, 46(1–3), 45–70. <https://doi.org/10.1016/j.compag.2004.11.001>
- Glover, P. W., & Déry, N. (2010). Streaming potential coupling coefficient of quartz glass bead packs: Dependence on grain diameter, pore size, and pore throat radius. *Geophysics*, 75(6), 1ND–Z138. <https://doi.org/10.1190/1.3509465>
- Guichet, X., Jouniaux, L., & Catel, N. (2006). Modification of streaming potential by precipitation of calcite in a sand–water system: Laboratory measurements in the pH range from 4 to 12. *Geophysical Journal International*, 166(1), 445–460. <https://doi.org/10.1111/j.1365-246X.2006.02922.x>
- Guichet, X., Jouniaux, L., & Pozzi, J. P. (2003). Streaming potential of a sand column in partial saturation conditions. *Journal of Geophysical Research: Solid Earth*, 108(B3). <https://doi.org/10.1029/2001JB001517>
- Han, T., Best, A. I., Sothcott, J., North, L. J., & MacGregor, L. M. (2015). Relationships among low frequency (2 Hz) electrical resistivity, porosity, clay content and permeability in reservoir sandstones. *Journal of Applied Geophysics*, 112, 279–289. <https://doi.org/10.1016/j.jappgeo.2014.12.006>
- Hayes, J. L., Riebe, C. S., Holbrook, W. S., Flinchum, B. A., & Hartsough, P. C. (2019). Porosity production in weathered rock: Where volumetric strain dominates over chemical mass loss. *Science Advances*, 5(9), eaao0834. <https://doi.org/10.1126/sciadv.aao0834>
- Hördt, A., Druiventak, A., Blaschek, R., Binot, F., Kemna, A., Kreye, P., & Zisser, N. (2009). Case histories of hydraulic conductivity estimation with induced polarization at the field scale. *Near Surface Geophysics*, 7(5–6), 529–545. <https://doi.org/10.3997/1873-0604.2009035>
- Jaafar, M. Z., Vinogradov, J., & Jackson, M. D. (2009). Measurement of streaming potential coupling coefficient in sandstones saturated with high salinity NaCl brine. *Geophysical Research Letters*, 36(21). <https://doi.org/10.1029/2009GL040549>
- Jackson, M. D., & Vinogradov, J. (2012). Impact of wettability on laboratory measurements of streaming potential in carbonates. *Colloids and Surfaces A: Physicochemical and Engineering Aspects*, 393, 86–95. <https://doi.org/10.1016/j.colsurfa.2011.11.005>
- Jardani, A., Revil, A., Barrash, W., Crespy, A., Rizzo, E., Straface, S., Cardiff, M., Malama, B., Miller, C., & Johnson, T. (2009). Reconstruction of the water table from self-potential data: A Bayesian approach. *Groundwater*, 47(2), 213–227. <https://doi.org/10.1111/j.1745-6584.2008.00513.x>
- Jardani, A., Revil, A., Santos, F., Fauchard, C., & Dupont, J. P. (2007). Detection of preferential infiltration pathways in sinkholes using joint inversion of self-potential and EM-34 conductivity data. *Geophysical Prospecting*, 55(5), 749–760. <https://doi.org/10.1111/j.1365-2478.2007.00638.x>
- Joseph, S., Ingham, M., & Gouws, G. (2016). Spectral-induced polarization measurements on sieved sands and the relationship to permeability. *Water Resources Research*, 52(6), 4226–4246. <https://doi.org/10.1002/2015WR018087>
- Jougnot, D., & Linde, N. (2013). Self-potentials in partially saturated media: The importance of explicit modeling of electrode effects. *Vadose Zone Journal*, 12(2), 1–21. <https://doi.org/10.2136/vzj2012.0169>
- Jougnot, D., Roubinet, D., Guarracino, L., & Maineuil, A. (2020). Modeling streaming potential in porous and fractured media, description and benefits of the effective excess charge density approach. In A. Biswas, & S. P. Sharma (Eds.), *Advances in modeling and interpretation in near surface geophysics* (pp. 61–96). Springer.
- Jouniaux, L., Maineuil, A., Naudet, V., Pessel, M., & Sailhac, P. (2009). Review of self-potential methods in hydrogeophysics. *Comptes Rendus Geoscience*, 341(10–11), 928–936. <https://doi.org/10.1016/j.crte.2009.08.008>
- Klein, K., & Santamarina, J. C. (1997). Methods for broad-band dielectric permittivity measurements (soil-water mixtures, 5 Hz to 1.3 GHz). *Geotechnical Testing Journal*, 20(2), 168–178.

- Koch, K., Kemna, A., Irving, J., & Holliger, K. (2011). Impact of changes in grain size and pore space on the hydraulic conductivity and spectral induced polarization response of sand. *Hydrology and Earth System Sciences*, 15(6), 1785–1794. <https://doi.org/10.5194/hess-15-1785-2011>
- Leroy, P., Revil, A., Kemna, A., Cosenza, P., & Ghorbani, A. (2008). Complex conductivity of water-saturated packs of glass beads. *Journal of Colloid and Interface Science*, 321(1), pp.103–117. <https://doi.org/10.1016/j.jcis.2007.12.031>
- Lesmes, D. P., & Friedman, S. P. (2005). Relationships between the electrical and hydrogeological properties of rocks and soils. In Y. Rubin & S. S. Hubbard, (Eds.), *Hydrogeophysics* (pp. 87–128). Springer.
- Lin, H. (2010). Earth's critical zone and hydrogeology: Concepts, characteristics, and advances. *Hydrology and Earth System Sciences*, 14(1), 25–45. <https://doi.org/10.5194/hess-14-25-2010>
- Linde, N., Jougnot, D., Revil, A., Matthäi, S. K., Arora, T., Renard, D., & Doussan, C. (2007). Streaming current generation in two-phase flow conditions. *Geophysical Research Letters*, 34(3), L03306. <https://doi.org/10.1029/2006GL028878>
- Mboh, C. M., Huisman, J. A., Zimmermann, E., & Vereecken, H. (2012). Coupled hydrogeophysical inversion of streaming potential signals for unsaturated soil hydraulic properties. *Vadose Zone Journal*, 11(2), vzj2011.0115. <https://doi.org/10.2136/vzj2011.0115>
- Mitchell, J. K., & Soga, K. (2005). *Fundamentals of soil behavior* (Volume 3). John Wiley & Sons.
- Mualem, Y. (1976). A new model for predicting the hydraulic conductivity of unsaturated porous media. *Water Resources Research*, 12(3), 513–522. <https://doi.org/10.1029/WR012i003p00513>
- Niu, Q., Fratta, D., & Wang, Y. H. (2015). The use of electrical conductivity measurements in the prediction of hydraulic conductivity of unsaturated soils. *Journal of Hydrology*, 522, 475–487. <https://doi.org/10.1016/j.jhydrol.2014.12.055>
- Paetzold, R. F., Matzkanin, G. A., & De Los Santos, A. (1985). Surface soil water content measurement using pulsed nuclear magnetic resonance techniques. *Soil Science Society of America Journal*, 49(3), 537–540. <https://doi.org/10.2136/sssaj1985.03615995004900030001x>
- Revil, A., & Florsch, N. (2010). Determination of permeability from spectral induced polarization in granular media. *Geophysical Journal International*, 181(3), 1480–1498.
- Revil, A., & Glover, P. W. J. (1998). Nature of surface electrical conductivity in natural sands, sandstones, and clays. *Geophysical Research Letters*, 25(5), 691–694. <https://doi.org/10.1029/98GL00296>
- Revil, A., & Jardani, A. (2013). *The self-potential method: Theory and applications in environmental geosciences*. Cambridge University Press.
- Revil, A., Kessouri, P., & Torres-Verdín, C. (2014). Electrical conductivity, induced polarization, and permeability of the Fontainebleau sandstone. *Geophysics*, 79(5), D301–D318. <https://doi.org/10.1190/geo2014-0036.1>
- Robinson, D. A., Lebron, I., Kocar, B., Phan, K., Sampson, M., Crook, N., & Fendorf, S. (2009). Time-lapse geophysical imaging of soil moisture dynamics in tropical deltaic soils: An aid to interpreting hydrological and geochemical processes. *Water Resources Research*, 45(4), W00D32. <https://doi.org/10.1029/2008WR006984>
- Schaap, M. G., & Leij, F. J. (2000). Improved prediction of unsaturated hydraulic conductivity with the Mualem-van Genuchten model. *Soil Science Society of America Journal*, 64(3), 843–851. <https://doi.org/10.2136/sssaj2000.643843x>
- Schön, J. H. (1996). *Physical properties of rocks: Fundamentals and principles of petrophysics* (Handbook of Geophysical Exploration, Seismic Exploration, Volume 18, pp. 379–478). Elsevier Science Ltd.
- Slater, L., Barrash, W., Montrey, J., & Binley, A. (2014). Electrical-hydraulic relationships observed for unconsolidated sediments in the presence of a cobble framework. *Water Resources Research*, 50(7), 5721–5742. <https://doi.org/10.1002/2013WR014631>
- Slater, L., & Lesmes, D. P. (2002). Electrical-hydraulic relationships observed for unconsolidated sediments. *Water Resources Research*, 38(10), 31–1. <https://doi.org/10.1029/2001WR001075>
- Sposito, G., Skipper, N. T., Sutton, R., Park, S. H., Soper, A. K., & Greathouse, J. A. (1999). Surface geochemistry of the clay minerals. *Proceedings of the National Academy of Sciences*, 96(7), 3358–3364. <https://doi.org/10.1073/pnas.96.7.3358>
- Take, W. A., & Bolton, M. D. (2003). Tensiometer saturation and the reliable measurement of soil suction. *Géotechnique*, 53(2), 159–172. <https://doi.org/10.1680/geot.2003.53.2.159>
- Topp, G. C., Davis, J. L., & Annan, A. P. (1980). Electromagnetic determination of soil water content: Measurements in coaxial transmission lines. *Water Resources Research*, 16(3), 574–582. <https://doi.org/10.1029/WR016i003p00574>
- Ulrich, C., & Slater, L. (2004). Induced polarization measurements on unsaturated, unconsolidated sands. *Geophysics*, 69(3), 653–861. <https://doi.org/10.1190/1.1759462>
- Urish, D. W. (1981). Electrical resistivity—Hydraulic conductivity relationships in glacial outwash aquifers. *Water Resources Research*, 17(5), 1401–1408. <https://doi.org/10.1029/WR017i005p01401>
- Valois, R., Cousquer, Y., Schmutz, M., Pryet, A., Delbart, C., & Dupuy, A. (2018). Characterizing stream-aquifer exchanges with self-potential measurements. *Groundwater*, 56(3), 437–450. <https://doi.org/10.1111/gwat.12594>
- van Genuchten, M. Th. (1980). A closed-form equation for predicting the hydraulic conductivity of unsaturated soils. *Soil Science Society of America Journal*, 44(5), 892–898. <https://doi.org/10.2136/sssaj1980.03615995004400050002x>
- Vinogradov, J., Jaafar, M. Z., & Jackson, M. D. (2010). Measurement of streaming potential coupling coefficient in sandstones saturated with natural and artificial brines at high salinity. *Journal of Geophysical Research: Solid Earth*, 115(B12). <https://doi.org/10.1029/2010JB007593>
- Vrugt, J. A., Gupta, H. V., Bouten, W., & Sorooshian, S. (2003). A shuffled complex evolution metropolis algorithm for optimization and uncertainty assessment of hydrologic model parameters. *Water Resources Research*, 39(8), 1201. <https://doi.org/10.1029/2002WR001642>
- Weller, A., Slater, L., Binley, A., Nordsiek, S., & Xu, S. (2015). Permeability prediction based on induced polarization: Insights from measurements on sandstone and unconsolidated samples spanning a wide permeability range. *Geophysics*, 80(2), D161–D173. <https://doi.org/10.1190/geo2014-0368.1>
- Wieting, C., Ebel, B. A., & Singha, K. (2017). Quantifying the effects of wildfire on changes in soil properties by surface burning of soils from the Boulder Creek Critical Zone Observatory. *Journal of Hydrology: Regional Studies*, 13, 43–57.
- Wösten, J. H. M., Pachepsky, Y. A., & Rawls, W. J. (2001). Pedotransfer functions: Bridging the gap between available basic soil data and missing soil hydraulic characteristics. *Journal of Hydrology*, 251(3–4), 123–150. [https://doi.org/10.1016/S0022-1694\(01\)00464-4](https://doi.org/10.1016/S0022-1694(01)00464-4)

- Wu, Y., Wang, Y. H., & Niu, Q. (2017). Integrating the Four-probe method and SWCC device to measure electrical resistivity anisotropy of unsaturated soil. *Geotechnical Testing Journal*, 40(4), 698–709. <https://doi.org/10.1520/GTJ20160160>
- Xie, J., Cui, Y., & Niu, Q. (2021). Coupled inversion of hydraulic and self-potential data from transient outflow experiments to estimate soil petrophysical properties. *Vadose Zone Journal*, 20(5), e20157. <https://doi.org/10.1002/vzj2.20157>
- Yang, C., Liu, S., Feng, Y., & Yang, H. (2018). Influence of electrode polarization on the potential of DC electrical exploration. *Journal of Applied Geophysics*, 149, 63–76. <https://doi.org/10.1016/j.jappgeo.2017.12.017>
- Yin, X., Gupta, V., Du, H., Wang, X., & Miller, J. D. (2012). Surface charge and wetting characteristics of layered silicate minerals.

*Advances in Colloid and Interface Science*, 179, 43–50. <https://doi.org/10.1016/j.cis.2012.06.004>

**How to cite this article:** Bienvenue, T., Xie, J., & Niu, Q. (2022). Developing a soil column system to measure hydrogeophysical properties of unconsolidated sediment. *Vadose Zone Journal*, 21, e20186. <https://doi.org/10.1002/vzj2.20186>